

The Mirroring of a Transient Regime of a Lathe Headstock Gearbox in the Evolution of Supplying Voltage of the AC Driving Motor

Neculai Eduard BUMBU

Technical University "Gheorghe Asachi" of Iasi, Romania, neculai-eduard.bumbu@student.tuiasi.ro

Mihaita HORODINCA

Technical University "Gheorghe Asachi" of Iasi, Romania, mihaita.horodince@academic.tuiasi.ro

Abstract

This paper aims to prove in experimental terms that a transient regime of a lathe headstock gearbox described by the evolution of the active electrical power absorbed by an AC driving motor supplied with a three phase electrical system is also quite well mirrored in the evolution of the root mean square of the electrical voltage measured at the motor input. A simple computer assisted setup and some relative simple techniques of active electrical power and electrical voltage monitoring are used for experimental purposes and signal numerical processing in a study of a transient regime characterized by a strong positive and negative absorbed active electrical power. This active electrical power is converted in active mechanical power requested by a transient regime of the gearbox, characterised by the increasing of speed (acceleration) and deceleration with electrically breaking (when the motor works as generator). It is proved that the evolution of the root mean square of the input voltage (on each of three phases) is related by the evolution of active electrical power with a simple equation. In this way it is possible to define a simple experimental technique to measure indirectly the active electrical power or the active mechanical power delivered by the rotor of an AC motor as well.

Keywords

lathe headstock gearbox, transient regime, AC motor, supplying voltage, monitoring

1. Introduction

An important approach in condition monitoring of the rotary machines (e. g. a machine-tool) driven by three phase AC motors is the evolution of the absorbed active electrical power (AEP). An AC motor works mainly as mechanical power supply and secondly as a mechanical power sensor. The evolution of the absorbed AEP is strictly related by the evolution of the active (real) mechanical power (AMP) [1, 2] delivered to driven rotary machine (AEP being almost proportional with AMP). Similarly, the active electrical energy (AEE) consumption is strictly related by the active mechanical energy (AME) [3, 4, 5].

Some computer aided AEP measurement techniques and methods on AC motors used for driving machine tools are available [6, 7, 8], for diagnosis and condition monitoring purposes, usually based on the evolution of instantaneous voltage and current delivered by the electrical supplying system. Frequently the AEP evolution is used for condition monitoring of the AC motor [9] (mechanical and electrical fault detection).

Some other papers focus on AEP and AEE evolution measurement for different electrical consumers (e.g. a household [10], a school [11]).

For a rotary machine driven by an AC motor supplied with a symmetrical three phase harmonic voltage system, the absorbed AEP is roughly defined as:

$$P = \frac{3 \cdot 2}{T} \int_{t=0}^{T/2} u(t) \cdot i(t) \cdot dt = 3 \cdot U \cdot I \cdot \cos(\varphi) \quad (1)$$

Here $u(t) = U\sqrt{2} \cdot \sin(\omega \cdot t)$ is the instantaneous voltage (IV) measured between a phase and the neutral wire, U being the voltage root mean square (VRMS) and ω being the angular frequency (related by the period T with $T=2\pi/\omega$). Also $i(t) = I\sqrt{2} \cdot \sin(\omega \cdot t - \varphi)$ is the instantaneous current (IC) circulating through the same phase, I being the root mean square of the current (CRMS), φ being the

phase shift between I_V and I_C and $\cos(\varphi)$ being the power factor (PF). In Eq. (1) $I \cdot \cos(\varphi)$ is also known as active current (AcC, [12]). According with Eq. (1) the AEP is the average value of the instantaneous power $p(t)=3 \cdot u(t) \cdot i(t)$ calculated on a semi-period $T/2$. There are $2/T$ AEP samples available in each second (or the AEP sampling rate is $2/T \text{ s}^{-1}$). A multiplication factor 3 is used in Eq. (1) because the I_V , I_C and PF are measured on a single phase. It is expected that the total delivered AEP is three times bigger than the AEP delivered by a single phase.

It is obvious that, according with Eq. (1), the AEP depends by VRMS, CRMS and PF or by VRMS and AcC as well. In theory for a constant VRMS value on each of the three phases which supply the AC motor, any variation of mechanical loading (mechanical power, AMP) at the motor rotor should be mandatory mirrored in the variation of CRMS and PF or the variation of AcC. It is expected that with a known value of VRMS (supposed to be constant) the value of AEP (calculated according with Eq. (1)) is determined by the values of CRMS and PF. It is well known from the literature that a variation of mechanical loading is mirrored in the variation of the CRMS [13] and the variation of PF as well [7].

This paper proves that the variation of the mechanical loading is sometimes also slightly mirrored in the evolution of VRMS measured at the AC motor electrical input. As a result, an easier way to measure indirectly the AMP (or AEP as well) is available: by measuring only the evolution of VRMS. There is a simple hypothesis to explain the VRMS variation due to AMP variation. This AMP variation produces a CRMS variation. The current on each phase circulates through an electrical wire with small resistance, so a small voltage drop (VD) occurs on this resistance according to Ohm's law. This VD diminishes the VRMS. Thus a variation of AMP implies a variation of AEP and CRMS which produces a variation of VD and VRMS. In other words, the variations of VRMS are related by AMP and AEP variation.

However we should mention that there is a severe limitation of this AMP (or AEP) measuring procedure: due to a very small resistance of electrical wires used to supply the AC motor, the VD and VRMS variations are also very small.

The next sections of this paper are focused on experimental setup description (Section 2), VRMS computer aided measurement and exploitation of the resources provided by VRMS evolution in time domain with discussions (Section 3) and conclusions (Section 4). For the experimental study a transient regime of a lathe headstock gearbox characterised by a strong variation of AEP was chosen.

2. Experimental Setup

The experimental setup is described in Figure 1a, being very similar with those already used before in [7]. There are also some similarities related by signal acquisition and data processing procedures already used before [7, 8].

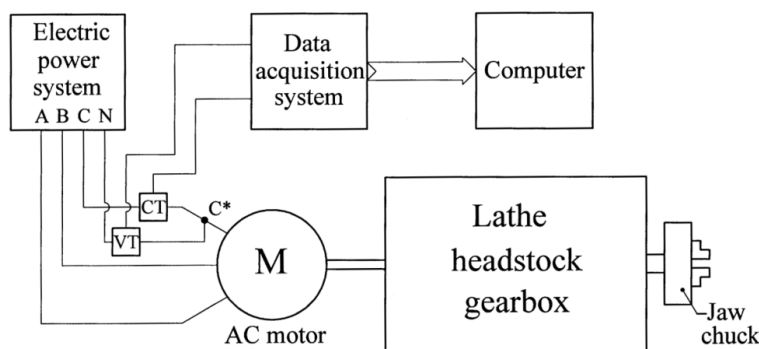


Fig. 1a. A formal description of the experimental setup

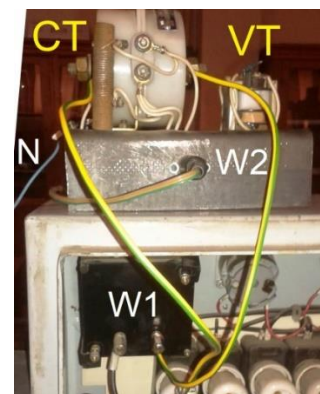


Fig. 1b. A view on CT and VT transformers with electrical wiring (partially)

An electric system with three phases (A, B, C and neutral wire N, with 50 Hz frequency) is used to supply the AC motor that drives the headstock gearbox of a Romanian SNA 360 lathe. On the phase C, a current transformer CT (depicted in Figure 1b) is placed. This transformer generates a description of I_C

(a voltage proportional with IC), delivered to a data acquisition system (an oscilloscope PicoScope 4424, from PicoTechnology, UK). A voltage transformer VT (depicted in Figure 1b) placed between the phase C and neutral wire N is used to measure the IV. This transformer generates a description of IV, delivered to the same oscilloscope. The numerical IV and IC evolutions in time domain are delivered by oscilloscope to a computer for data processing and signal analysis purposes. The theoretical approach used to find-out the evolution of AEP mainly based on a numerical approximation of the integral from Eq. (1), briefly presented here below, was already described before [7, 8].

With n samples of IV and n samples of IC on a semi-period $T/2$ (a generic IV sample is written as $u[t_k]$ and a generic IC sample is written as $i[t_k]$, with t_k as sampling time) and Δt being the sampling period (with $n \cdot \Delta t = T/2$), the approximate expression of AEP from Eq. (1), calculated on a semi period $T/2$ is written as:

$$P = \frac{3 \cdot 2}{T} \int_{t=0}^{T/2} u(t) \cdot i(t) \cdot dt \approx \frac{3}{n \cdot \Delta t} \sum_{k=1}^{k=n} u[t_k] \cdot i[t_k] \cdot \Delta t = \frac{3}{n} \sum_{k=1}^{k=n} u[t_k] \cdot i[t_k] \quad (2)$$

In Eq. (2) the sampling time t_k is described as $t_k = k \cdot \Delta t$ and $dt \approx \Delta t$.

Some supplementary approaches related by IV signal processing (e.g. the VRMS description) will be introduced in Section 3.2 of this paper.

The kinematics of the lathe headstock gearbox is described in Figure 2. An asynchronous three phase AC motor (5.5 kW, 1500 rpm, earlier introduced in Figure 1) drives the lathe headstock gearbox. This gearbox uses two driving flat belts transmissions. In order to change the rotational speed some movable gears, some fixed gears and three electromagnetic clutches (EMC1, EMC2 and EMC3) placed on the shaft I are used. The kinematic configuration described in Figure 2 assures a rotational speed of 1624.3 rpm at spindle (the output). On the shaft I only the EMC2 is engaged.

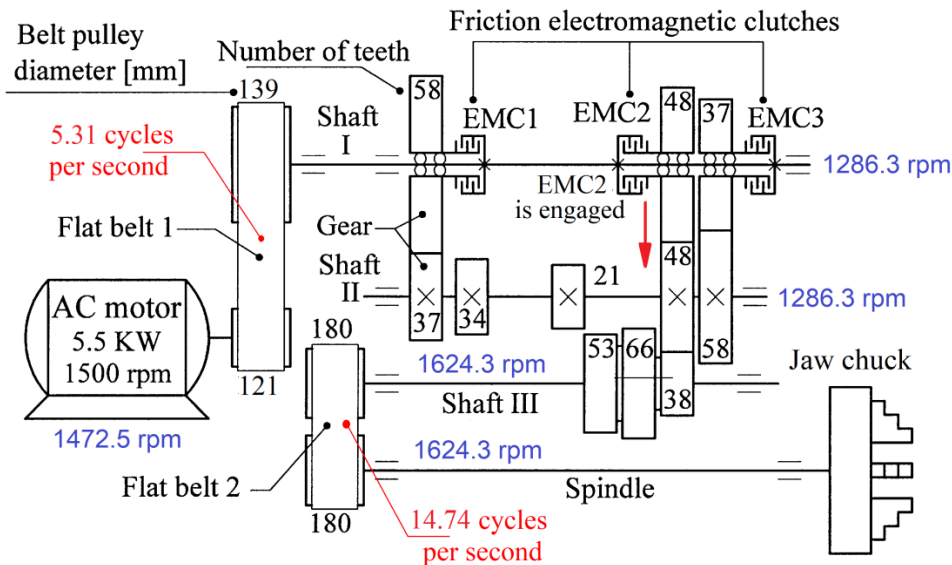


Fig. 2. A description of the lathe headstock gearbox kinematics

The three electromagnetic clutches allow generating the transient regimes (by clutch engaging and disengaging, with AC motor running with a rotational speed slightly depending by loading).

3. Experimental Results and Discussion

3.1. A transient regime described by the evolution of the active electric power

Let's consider a transient regime of lathe headstock gearbox during a period of 50 s, described by AEP evolution from Figure 3 and some comments about this. With 50 Hz frequency of instantaneous voltage, $T = 1/50$ s, $2/T = 100$ s⁻¹ (the sampling rate of AEP being $2/T$) there are 5000 AEP samples, with $n = 1000$ (and $\Delta t = 10$ μ s).

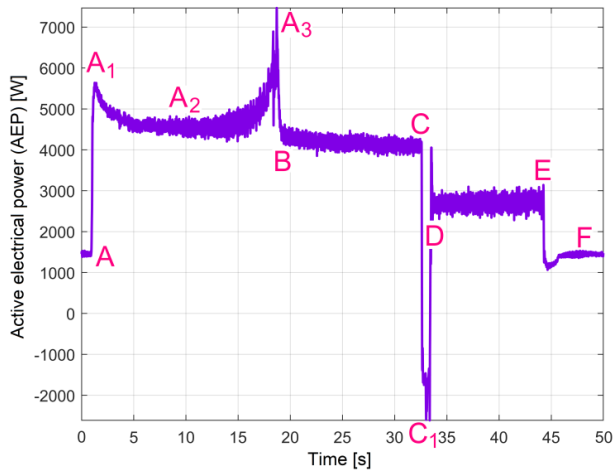


Fig. 3. A description of a transient regime in AEP evolution

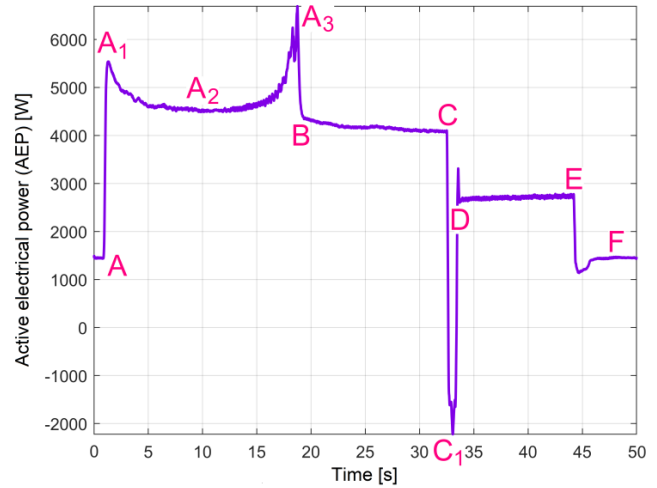


Fig. 4. A description of the AEP from Figure 3 using a low pass filter

In the beginning, the AC motor is already on; all the electromagnetic clutches are disengaged. The AC motor rotates only the first belt transmission and the shaft I. The AC motor delivers 1450 W of AEP. The transient regime starts (label A on Figure 3) when the electromagnetic clutch EMC2 is engaged.

Due to the acceleration of headstock gearbox rotation parts (and mechanical inertia as well) for a period of time (between A and B) there is an important AMP variation (and AEP as well). A strong sliding phenomenon in belt transmission occurs (and probably also in the electromagnetic clutch EMC2). In A₁ the sliding starts, in A₃ the sliding ceases. Between A₁ and A₂ the absorbed AEP first decreases until a relative stationary operating regime in A₂ (because of sliding, the belt heats up and the mechanical stress in belt decreases, the torque transmitted by belt-pulley friction also decreases). Between A₂ and A₃ the sliding decreases, a strong AEP peak is produced in A₃ (7460 W). The acceleration of the headstock gearbox ceased in B and here starts a relative stationary operating regime, the spindle rotates with constant rotational speed (1624.3 rpm, measured using a method exposed in [14]). Now the absorbed AEP (4200 W in average) is converted mainly in AMP which is used to turn the rotary parts of the headstock gearbox running idle. This AMP is totally converted in heating (by dry and viscous friction).

In C the kinematic configuration is suddenly changed (EMC2 is disengaged and EMC3 is engaged) in order to obtain a smaller rotational speed at spindle (1042.2 rpm). A new transitory phenomenon is produced. The AEP drops temporary, with a negative peak at -2610 W in C₁. For a short time, the headstock gearbox works as AMP supply for AC motor, until the supplementary kinetic energy is eliminated. Now the motor works as a brake for gearbox and as a generator as well, it converts the AMP in AEP which temporary flows from motor to electric power system, in opposite direction to the normal one. That is why in C₁ the absorbed AEP is negative.

In D the new transitory phenomena ceased, a new relative stationary operating regime starts, the spindle rotates constantly on 1042.2 rpm, with 2700 W average AEP consumption. In E the clutch EMC3 is disengaged, a part of headstock gearbox is not mechanical supplied anymore, the spindle stops and the absorbed AEP drops (in F) to the value had before A.

The AEP evolution between B and C or between D and E is very useful for headstock gearbox condition monitoring (by conversion of AEP evolution from time to frequency domain, e.g. by fast Fourier transform, FFT). A better approach on AEP evolution from Figure 3 is provided by AEP low pass numerical filtering as Figure 4 shows. A moving average filter was used (with 15 samples in the average). Because of numerical filtering, the AEP amplitude in peaks decrease (e.g. in A₃ and in C₁).

3.2. An approach on the evolution of instantaneous voltage during the transient regime

A partial description of the instantaneous voltage evolution having the VRMS amplitude (as $u^*(t)=U \cdot \sin(\omega \cdot t)$ and $u(t)=u^*(t) \cdot \sqrt{2}$) during the transient regime already depicted before in AEP evolution (Figures 3 and 4) is done in Figure 5 (in numerical format $u^*[t_k]$). Here only the area of the

maximum values on the positive alternation of $u^*[t_k]$ was represented. As is clearly indicated on Figure 5, there is an evident relationship between the AEP and instantaneous voltage evolution with VRMS amplitude (and $u(t)$ as well): the increasing of absorbed AEP diminishes the instantaneous voltage. This is because the voltage drop on the wire on phase C (the part formally placed between C and C*, Figure 1a) increases. A part of this wire is depicted as W1 in Figure 1b (here a copper wire with 4 mm diameter and 0.6 m length). For this experiment this part W1 was temporary replaced with a 1 mm diameter and 5 m length wire (a bigger resistance of wire W increases the voltage drop).

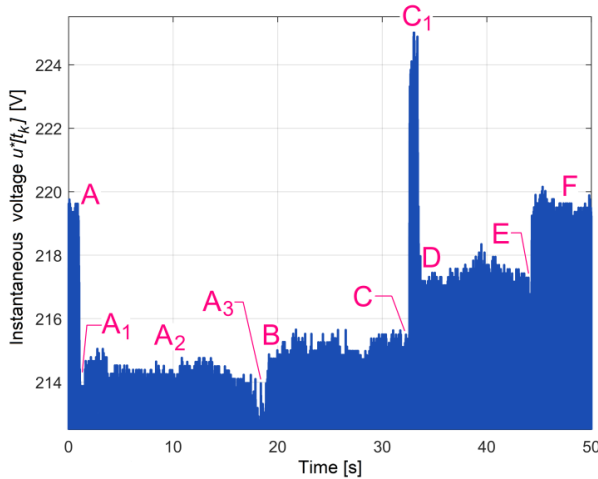


Fig. 5. A partial description of the instantaneous voltage $u^*[t_k]$ evolution during the transient regime

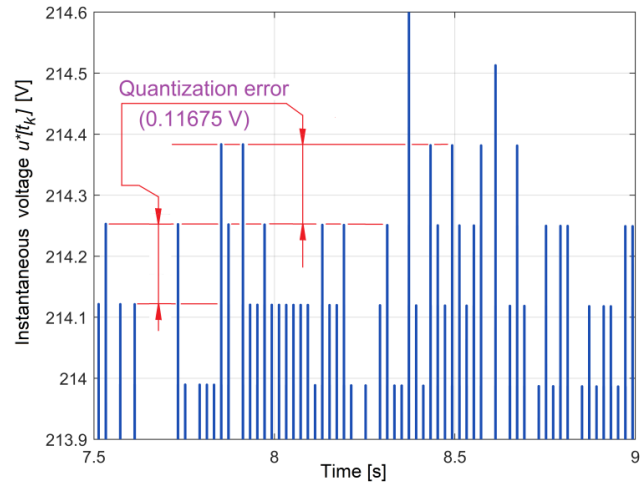


Fig. 6. A zoom in detail in area A₂ of Figure 5 with highlighting of the quantization error on $u^*[t_k]$ evolution

Figure 6 presents a zoom in detail of Figure 5 (in A₂ area). Due to a relative small analog to digital conversion (ADC) resolution of the numerical oscilloscope (12 bits) and a high full scale voltage range (from -239.12 V up to 239.12 V) there is a relative big ADC voltage resolution Δu revealed on Figure 6 as voltage quantization error Q_{Ve} (with $Q_{Ve} = \Delta u = 0.11675$ V). Here $u^*[t_k]$ is described as $u^*[t_k] = g \cdot \Delta u [k \cdot \Delta u]$, with g an integer between -2^{11} and $+2^{11}$. This quantization error is a relative inconvenient, acting in negative way on the quality of the mirroring of the AEP evolution on VRMS evolution. A higher ADC resolution (e. g. 16 bits) reduce significantly this inconvenient (for 16 bits $Q_{Ve} = 72.973$ μ V). However for AEP evolution the VRMS quantization error doesn't have a strong negative effect because the current quantization error Q_{Ie} is very small ($Q_{Ie} = 0.00933$ A). According with the second part of Eq. (1) the AEP quantization error Q_{AEPe} should be roughly defined as $Q_{AEPe} = Q_{Ve} \cdot Q_{Ie} = 0.001089$ W, if the power factor quantization error (surely smaller than 1) is neglected.

3.3. An approach on the evolution of VRMS during the transient regime

The VRMS evolution of the signal described in Figure 5 is the envelope of $u^*[t_k]$ signal, as instantaneous amplitude evolution. The maximum value of u^* on each positive alternation (and its time) describes a sample U of VRMS, with T as sampling period (so with $1/T = 50$ s⁻¹ as sampling rate or sampling frequency). A better approach is available if $u^*[t_k]$ signal is replaced by $|u^*(t_k)|$ signal (all the alternations of $|u^*(t_k)|$ are positive). The maximum value of $|u^*|$ on each alternation (and its time) describes also a sample of VRMS, with $T/2$ as sampling period (so with $2/T = 100$ s⁻¹ as sampling rate or sampling frequency, two times bigger than before).

There are two steps in signal processing in order to obtain the VRMS from $|u^*(t_k)|$ evolution.

1. Firstly it is necessary to detect the limits of each alternation. Each two successive zero-crossing moments (t_j, t_{j+1}) of $u^*[t_k]$ describes the limits of an alternation (positive or negative). The detection techniques of these zero-crossing moments were fully explained before in [14]. Because of electrical noise, frequently some false zero-crossing occur on $u^*[t_k]$ evolution, as Figure 7 indicates (a very short detail in the moment of C area, as a red coloured curve, with seven false zero-crossing, f_1, f_2, \dots, f_7). This electric noise is generated when the coil of the EMC3 clutch is switched on. The easiest way

to eliminate the false zero-crossing events is to use a low-pass numerical filter (e. g. a moving average filter) for $u^*[t_k]$ signal (the green coloured curve on Figure 7, with 12 points in the average). There is a single zero-crossing on the $u^*[t_k]$ filtered signal (conventionally defined at time t_j). A zoom-out of Figure 7 is given in Figure 8. The electrical noise area from Figure 7 is revealed in EN₂ area of Figure 8. There is also another electrical noise area EN₁ before EN₂ generated when the coil of EMC₂ clutch is disconnected. This EN₂ area has also a bad influence on VRMS detection if the $u^*[t_k]$ signal is not filtered.

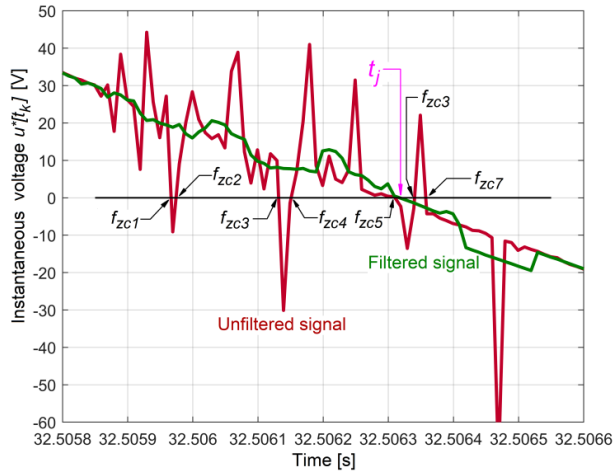


Fig. 7. Zero-crossing detection on $u^*[t_k]$ signal with electrical noise

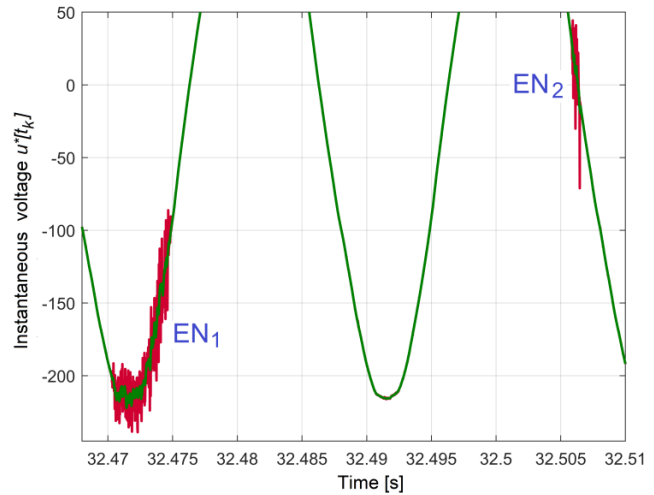


Fig. 8. Electrical noise areas on unfiltered (in red) and filtered (in green) signal $u^*[t_k]$

2. Secondly the $u^*[t_k]$ filtered signal should be converted in $|u^*(t_k)|$ signal. All the alternations of $u^*[t_k]$ become positive. The zero-crossing limits of each alternation (t_j, t_{j+1}) determined before for $u^*[t_k]$ filtered signal are available also for $|u^*(t_k)|$ signal. According with Figure 9 (which shows an alternation on $|u^*(t_k)|$ signal in A₂ area of Figure 5) each alternation describes a VRMS sample $U_m[t_m]$, with U_m as the maximum value of filtered $|u^*(t_k)|$ signal on that alternation and with $t_m = (t_j + t_{j+1})/2$ as the sample time (it is expected that the maximum value is placed in the middle of the range $t_j - t_{j+1}$). Each $t_{m+1} - t_m$ difference can be expressed approximately as $t_{m+1} - t_m \approx T/2$.

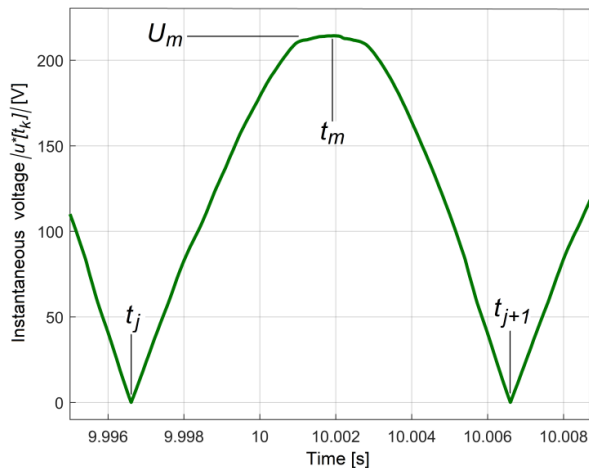


Fig. 9. The description of a VRMS sample

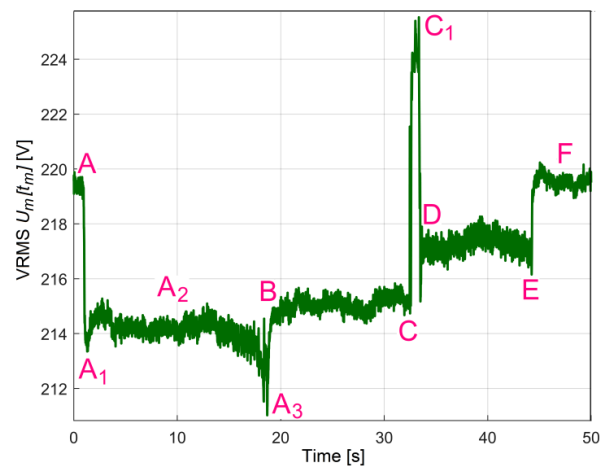


Fig. 10. The VRMS signal evolution ($U_m[t_m]$)

Figure 10 shows the VRMS signal evolution ($U_m[t_m]$) during the transient regime, determined by the procedure described above. Apparently there is a noisy signal. A deeper analysis proves that this strong variation of VRMS signal (especially between B and C or between D and E areas) is useful for condition monitoring and diagnosis of headstock gearbox (e.g. by VRMS spectrum analysis using FFT).

This will be a future challenge of our work.

Figure 11 shows the same evolution of the VRMS signal but deduced from unfiltered $u^*[t_k]$ signal. As expected, some false zero-crossing events imply a wrong description of the VRMS. By comparison between Figures 11 and 10, it is clear that the numerical filtering of $u^*[t_k]$ signal has a positive effect in false zero-crossing events removing and produce a correct description of VRMS. The peak from C* on Figure 11 is generated by the electrical noise from EN₁ area (from Figure 8). It is strongly reduced by filtering in Figure 10.

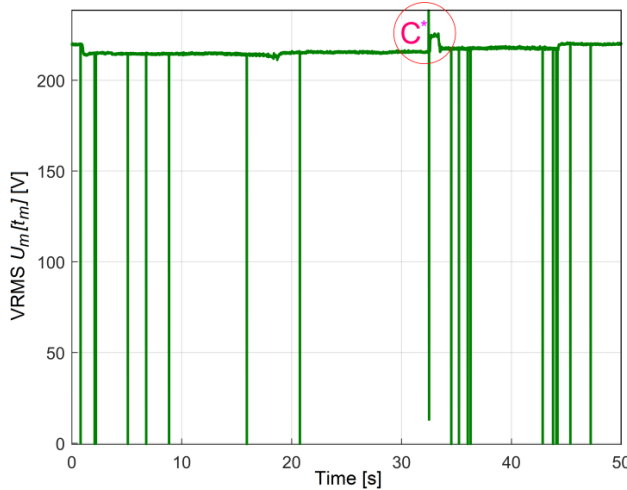


Fig. 11. A wrong described VRMS signal evolution ($U_m[t_m]$) caused by false zero-crossing

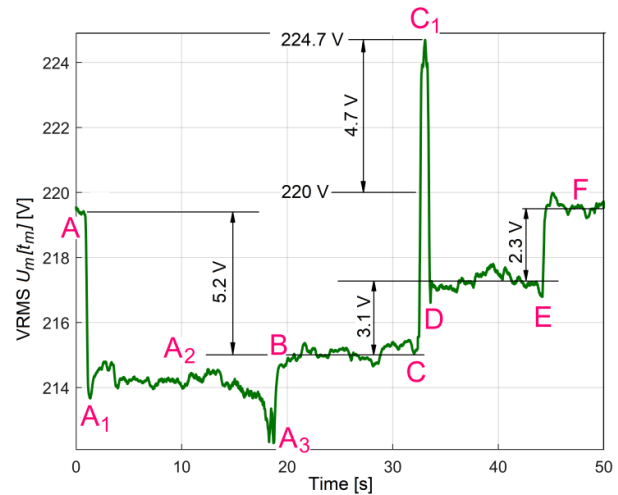


Fig. 12. The low-pass numerical filtered VRMS signal evolution ($U_m[t_m]$)

The relative noisy evolution of VRMS from Figure 10 can be strongly attenuated also by numerical filtering. Figure 12 shows the low-pass numerical filtered VRMS signal evolution ($U_m[t_m]$). A moving average filter (with 20 samples in the average) was used. There is an interesting remark here: in the area between C and D the strong positive peak of VRMS (in C₁) describes the behaviour of AC motor as generator, the AEP is negative (the AEP flows in inverse direction, from AC motor to electric power supply), the VRMS is bigger that the average root means square of the voltage on phase C without AC motor (with a 220 V value).

Now a comparison between Figures 12 and 4 clearly shows that the evolution of VRMS is related by the evolution of AEP. Even more, there is a relationship between VRMS and AEP. If we accept a description of an AEP sample as $P_m[t_m]$ then this relationship can be written as:

$$P_m[t_m] \approx -C_1(U_m[t_m] - C_2) \quad (3)$$

In Eq. (3) $C_1 = 645.9 \text{ W/V}$ and $C_2 = 218.416 \text{ V}$. This relationship is confirmed by Figure 13. The left- hand side of Eq. (3) is depicted with blue (a description already given in Figure 4) the right-side is depicted with green (this last description is generated by calculus from the evolution given in Figure 12).

The curves fit quite well. There is a simple explanation about the differences between the curves from Figure 13: as clearly was proved, the variation of VRMS is related by AEP through the mechanical loading (AMP) of the AC motor, but is also related by electric power system used to supply the AC motor. The VRMS of the voltage delivered by this system (here on phase C) when the AC motor is removed is not strictly constant (at 220 V) as expected. This is clear depicted on Figure 14. The green coloured curve is the VRMS already given in Figure 12; the one coloured in blue is the VRMS evolution without the AC motor. There is a 1.2 V peak to peak variation. Probably other electric consumers (e. g. some other AC motors) placed somewhere far away on the same phase C acts in the same way as our AC motor during transient regimes.

A new experiment related by the mirroring of the same transient regime in VRMS evolution was done. This time the original part of the wire W1 for electrical wiring of transformers was used (Figure 1b, a copper wire with 4 mm diameter and 0.6 m length). A smaller electrical resistance of the wire should

produces a smaller voltage drop VD so a smaller variation of VRMS. This is confirmed on Figure 15 (the equivalent of Figure 12). Because the gearbox is colder than before, the transient regime between A₁ and A₃ is significantly longer.

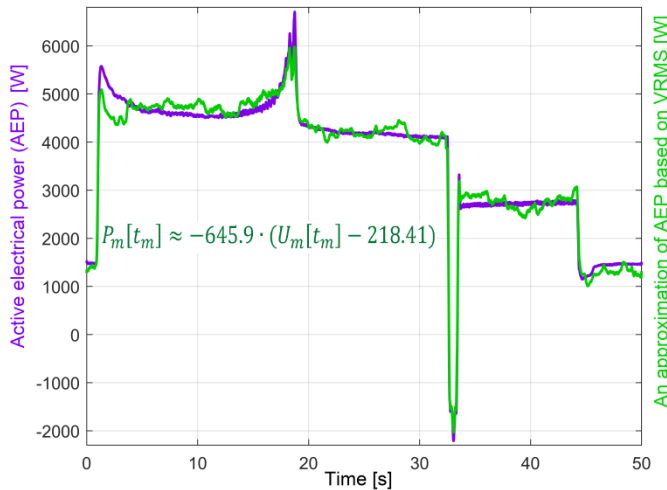


Fig. 13. A description of AEP from Figure 4 (blue curve) based on VRMS evolution (green curve)

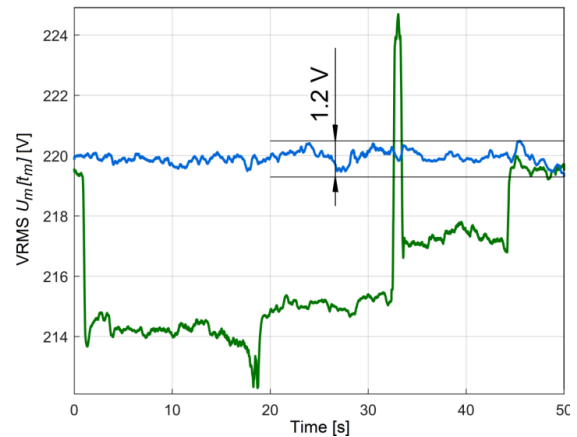


Fig. 14. A description of VRMS on phase C during transient regime (green curve) and without any electrical consumer (blue curve)

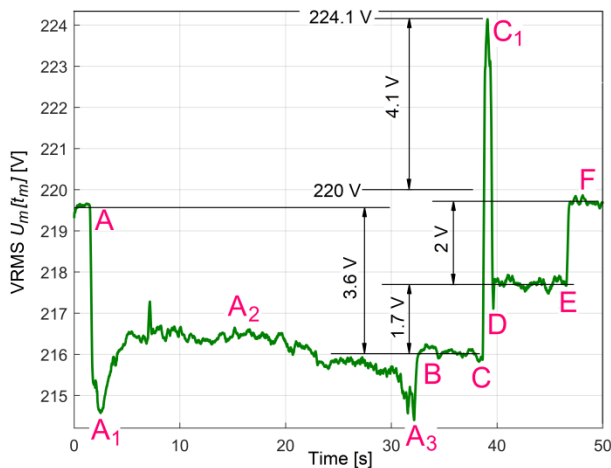


Fig. 15. The low-pass numerical filtered VRMS signal evolution ($U_m[t_m]$) during a new experiment with transient regime

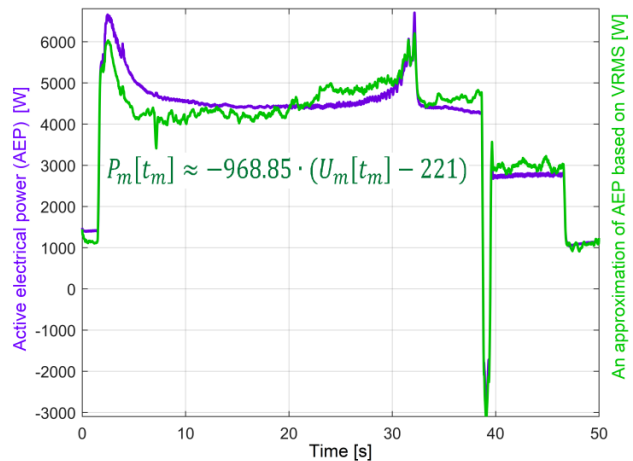


Fig. 16. A description of AEP (blue curve) based on VRMS evolution (green curve), during the transient regime described in Figure 15

The description of AEP using the VRMS evolution (in similarly manner with Figure 13) is given in Figure 16. The correlation between AEP and VRMS is described by the same Eq. (3), this time C_1 being bigger than before ($968.85 > 645.9$) of course because the electrical resistance of the original part of the wire W1 is smaller than before (the voltage drop VD decreases for the same AEP variation). Because C_1 increases, the fitting between curves in Figure 16 is worse than in Figure 13.

It is clear that this part of wire W1 (and also all the wires between C and C* on Figure 1a as well) acts as a shunt resistor. If the second part of the Eq. (1) is used to describe the AEP ($P=3 \cdot U \cdot I \cdot \cos(\varphi)$) than the VRMS U should be mandatory measured (the hypothesis that VRMS U is constant is false, as it was proved in this paper). Alternatively the evolution of VRMS can be used as an indirect way for AEP evolution description, as Figure 12 and 16 proves. In this case a higher ADC resolution is probably necessary (with 14 or 16 bits). Eventually a small increasing of the shunt resistor (the resistance of the wire between C and C* on Figure 1a) increases also the sensitivity $1/C_1$ of VRMS measurement (because C_1 from Eq. (3) decreases).

4. Conclusions and Future Work

The main conclusion of this research is that the VRMS on each of three phases of an electric system supplying an AC motor used to drive a rotary machine (here a lathe headstock gearbox) is variable (despite that in a common approach, VRMS is considered constant), especially in transient regimes characterized by a strong variation of absorbed AEP or delivered AMP as well. There is a relative quite well established correlation (relationship) between AEP and VRMS.

There are two consequences here. Firstly (as a negative one) in classical way of AEP measurement (based on the equation $P=3 \cdot U \cdot I \cdot \cos(\varphi)$), all three involved variables: VRMS (U), CRMS (I) and PF ($\cos(\varphi)$) should be measured before calculus of P . Secondly (as a positive consequence) a new approach is available in transient regimes monitoring and indirect AEP measurement, based on the VRMS evolution (the measurement of VRMS is simpler than the AEP measurement).

This conclusion is a result of some experimental approaches based on a computer aided measurement setup and signal processing procedures (for AEP and VRMS measurement and monitoring). A transient regime with strong variation of AEP was chosen. A relationship between AEP and VRMS was established and experimentally proved.

Some supplementary resources of VRMS evolution are available for a future research. An interesting hypothesis will be to explore the resources of VRMS evolution in frequency domain for condition monitoring (diagnosis) purposes. There is a simple reason for this hypothesis: any damaged rotary part inside the headstock gearbox needs frequently to be supplied with a variable component of the total AEP. This variable component can be identified directly using the evolution in frequency domain of AEP or indirectly using the evolution of VRMS. At least the amplitudes and the frequencies of fundamentals and harmonics of these variable components should be determined by analysis in frequency domain, e. g. by FFT.

A further approach will be focused to reveal the resources of evolution of CRMS and PF during the same transient regime.

All the conclusions and the considerations above are available for any machine or equipment driven with an AC motor.

References

- Liu P., Liu F., Liu G. (2017): *A new approach for calculating the input power of machine tool main transmission systems*. Advances in Mechanical Engineering, ISSN1687-8140, Vol. 9, No. 9, pp. 1-10, <https://doi.org/10.1177/1687814017723791>
- Miura K., Döbbeler B., Klocke F. (2018): *Cutting power estimation via external voltage and current sensors on, feed-drive axis for the straight milling process*. Procedia CIRP, ISSN 2212-8271, Vol. 78, pp. 323-328, <https://doi.org/10.1016/j.procir.2018.09.068>
- Abdoli S., Semere Tesfamariam D. (2014): *Investigation on machine tools energy consumptions*. International Journal of Mechanical, Aerospace, Industrial and Mechatronics Engineering, ISSN 2077-124X, Vol. 8, No. 6, pp.1091-1098, <http://urn.kb.se/resolve?urn=urn:nbn:se:kth:diva-219596>
- Haas F., Suárez A., Cus F., Zuperl U. (2019): *Platform for monitoring and comparing machining processes in terms of energy efficiency*. Transactions of FAMENA, ISSN 1333-1124, Vol. XLIII, No. 2, pp. 31-47, <https://hrcak.srce.hr/223163>
- Hussain T., Ullah F.U.M., Muhammad K., Rho S., Ullah A., Hwang E., Moon J., Baik S.W. (2021): *Smart and intelligent energy monitoring systems: A comprehensive literature survey and future research guidelines*. International Journal of Energy Research, ISSN 1099-114X, Vol. 45, pp. 3590-3614, <https://doi.org/10.1002/er.6093>
- Huzlík R., Blecha P., Vašíček A., Houška P., Holub M. (2014): *Device for measuring of active power and energy at machine tools*. In Březina T, Jabłoński R. (eds): Mechatronics 2013. Recent Technological and Scientific Advances, ISBN 978-3-319-02294-9, pp. 503-509, <https://link.springer.com/book/10.1007/978-3-319-02294-9>
- Horodincea M. (2016): *The monitoring of transient regimes on machine tools based on speed, acceleration and active electric power absorbed by motors*. ModTech 2016, IOP Conference Series: Materials Science and Engineering, Vol. 145, is. 2, <https://iopscience.iop.org/article/10.1088/1757-899X/145/2/022026/meta>
- Chifan F., Luca C., Horodincea M., Dumitras C.G. (2019): *An Approach on a Transient Regime of a CNC Machining Center Spindle Drive System Using the Active Electrical Power Evolution*. RECENT, ISSN 1582-0246, Vol. 20, no. 3(59), pp. 99-106, <https://doi.org/10.31926/RECENT.2019.59.099>
- Bazan G.H, Goedel A., Duque-Perez O., Morinigo-Sotelo D. (2021): *Multi-fault diagnosis in three-phase induction motors using data optimization and machine learning techniques*. Electronics, ISSN 2079-9292, Vol. 10, no.

- 1462, pp. 1-23, <https://doi.org/10.3390/electronics10121462>
10. Cannas B., Carcangiu S., Carta D., Fanni A., Muscas C., Sias G., Canetto B., Fresi L., Porcu P. (2021): *NILM techniques applied to a real-time monitoring system of the electricity consumptions*. ACTA IMEKO, ISSN 2221-870X, Vol. 10, no. 2, pp. 139-146, http://dx.doi.org/10.21014/acta_imeko.v10i2.1054
 11. Anggraini D., Effendy N., Al Hafiz M.I., Luviano D.O. (2018): *Research and development of a power monitoring system for the sustainable energy management system implementation at green school, Bali, Indonesia*. E3S Web Conf., ISSN 2267-1242, Vol. 43, ASTECHNOVA 2017 International Energy Conference, <https://doi.org/10.1051/e3sconf/20184301021>
 12. Willems J.L. (2007): *Active current, reactive current, Kirchhoff's laws and Tellegen's theorem*. Electrical Power Quality and Utilisation Journal, ISSN 1896-4672, Vol. XIII, no. 1, pp. 5-8, <https://www.researchgate.net/publication/294124832>
 13. Ottewill J.R., Orkisz M. (2013): *Condition monitoring of gearboxes using synchronously averaged electric motor signals*. Mechanical Systems and Signal Processing, ISSN 0888-3270, Vol. 38, No. 2, p. 482-498, <https://doi.org/10.1016/j.ymssp.2013.01.008>
 14. Horodincea M., Ciurdea I., Chitariu D.-F., Munteanu A., Boca M. (2020): *Some approaches on instantaneous angular speed measurement using a two-phase n poles AC generator as sensor*. Measurement, ISSN 0263-2241, Vol. 157, pp. 1-13, <https://doi.org/10.1016/j.measurement.2020.107636>